HHS Public Access

Author manuscript

Cancer Res. Author manuscript; available in PMC 2022 May 04.

Published in final edited form as:

Cancer Res. 2021 July 01; 81(13): 3649–3663. doi:10.1158/0008-5472.CAN-20-1799.

Phenotypic heterogeneity and metastasis of breast cancer cells

Lauren A. Hapach[1,2], **Shawn P. Carey**[1], **Samantha C. Schwager**[2], **Paul V. Taufalele**[2], **Wenjun Wang**[2], **Jenna A. Mosier**[2], **Nerymar Ortiz-Otero**[1], **Tanner J. McArdle**[3], **Zachary E. Goldblatt**[1], **Marsha C. Lampi**[1], **Francois Bordeleau**[2,4], **Jocelyn R. Marshall**[1], **Isaac M. Richardson**[2], **Jiahe Li**[1], **Michael R. King**[2], **Cynthia A. Reinhart-King**[2,*]

[1]Nancy E. and Peter C. Meinig School of Biomedical Engineering, Cornell University, Ithaca, NY, 14853, USA

[2]Department of Biomedical Engineering, Vanderbilt University, Nashville, TN, 37212

[3]School of Medicine, Vanderbilt University, Nashville, TN, 37212

[4]CHU de Québec-Université Laval Research Center, Université Laval Cancer Research Center, Québec, Canada, G1R 3S3

Abstract

While intratumoral genomic heterogeneity can impede cancer research and treatment, less is known about the effects of phenotypic heterogeneities. To investigate the role of cell migration heterogeneities in metastasis, we phenotypically sorted metastatic breast cancer cells into two subpopulations based on migration ability. While migration is typically considered to be associated with metastasis, when injected orthotopically in vivo, the weakly migratory subpopulation metastasized significantly more than the highly migratory subpopulation. To investigate the mechanism behind this observation, both subpopulations were assessed at each stage of the metastatic cascade, including dissemination from the primary tumor, survival in the circulation, extravasation, and colonization. While both subpopulations performed each step successfully, weakly migratory cells presented as circulating tumor cell (CTC) clusters in the circulation, suggesting clustering as one potential mechanism behind the increased metastasis of weakly migratory cells. RNA sequencing revealed weakly migratory subpopulations to be more epithelial and highly migratory subpopulations to be more mesenchymal. Depletion of E-cadherin expression from weakly migratory cells abrogated metastasis. Conversely, induction of E-cadherin expression in highly migratory cells increased metastasis. Clinical patient data and blood samples showed that CTC clustering and E-cadherin expression are both associated with worsened patient outcome. This study demonstrates that deconvolving phenotypic heterogeneities can reveal fundamental insights into metastatic progression. More specifically, these results indicate that migratory ability does not necessarily correlate with metastatic potential, and that E-cadherin

[*]**Corresponding author:** Cynthia A. Reinhart-King, Department of Biomedical Engineering, Vanderbilt University, Nashville, TN, 37212, cynthia.reinhart-king@vanderbilt.edu, Phone: (615)-875-8309).

Author Contributions

Conceptions and Design: L.A.H., S.P.C., F.B., M.R.K., and C.A.R.-K.

Acquisition of Data: L.A.H, S.P.C., Z.E.G., S.C.S., W.W., P.V.T, M.C.L., N.O.-O., J.A.M., F.B., J.R.M., and J.L.

Analysis of Data: L.A.H., S.P.C., Z.E.G., S.C.S., W.W., M.C.L., P.V.T., J.A.M., T.J.M., N.O.-O., and I.M.R. Writing of the manuscript: L.A.H. and C.A.R-.K.

Conflict of Interest: The authors declare no potential conflicts of interest.

promotes metastasis in phenotypically-sorted breast cancer cell subpopulations by enabling CTC clustering.

Keywords

cell migration; circulating tumor cells (CTCs); breast cancer; invasive ductal carcinoma (IDC); epithelial to mesenchymal transition (EMT)

Introduction

Genetic and epigenetic subclones generated within the primary tumor generate significant phenotypic diversity that greatly complicates cancer diagnosis and treatment (1). Intratumor heterogeneity has been identified as a prognostic marker associated with decreased patient survival (2), and it can obscure the most aggressive drivers of cancer migration and metastasis (3–5). Subclones that ultimately drive disease progression may be present in the primary tumor at the time of diagnosis in almost undetectable amounts (1). If these important metastatic subclones could be identified and targeted early, patient outcomes would greatly improve. As metastasis is a complex, multi-step process, parsing apart the phenotypes which can complete the entire metastatic cascade is critical to improving therapeutic strategies. While much has been done to elucidate which cellular properties endow tumor cells with the ability to perform the various steps of the metastatic cascade, it remains unclear whether success in one part of the metastatic cascade is indicative of success in others (5).

As tumor cell infiltration into the surrounding stroma is an early step in cancer metastasis, tumor cell migration has been considered essential for cancer malignancy (6). However, clinical evidence as well as in vitro and in vivo studies indicate that heterogeneity exists in cancer cell migration ability and mode, both between and within individual tumors (7). This range of migratory phenotypes is thought to be partially due to the crosstalk between cancer cells and the tumor stroma, where extracellular matrix (ECM) architectural features can induce specific migratory behaviors (8–11). While ECM features can account for part of the heterogeneity observed in local tumor dissemination, less is known regarding how tumor-intrinsic phenotypic heterogeneity impacts cancer cell migration and ultimately, metastasis.

To address intratumor heterogeneity of cellular migration behaviors and isolate the role of migration in metastasis, we sorted metastatic cells based on their ability to migrate, one of the earliest proposed requirements for metastatic progression (12,13). While migration is believed to be correlated with metastasis, when these subpopulations were used in an orthotopic metastasis model, the poorly migratory subpopulation readily colonized distal locations including lungs, liver, and bone, while the highly migratory cells showed poor metastatic potential in all tissues. Our data indicate that E-cadherin is essential to the metastatic fitness of the weakly migratory subpopulation, and the highly migratory subpopulation can be rescued with induction of E-cadherin expression. In patient samples, circulating tumor microemboli concentration and patient survival time are correlated, and we observed that circulating tumor cells in metastatic breast cancer samples were E-cadherin

positive. Together, these findings indicate that in vitro migration ability does not necessarily correlate with metastatic capability, and E-cadherin is a major driver of the metastatic phenotype.

Materials and Methods

Cell culture

MDA-MB-231 cells (ATCC Cat# HTB-26), HEK293T cells (ATCC Cat# CRL-3216), HUVECs (Lonza), MCF10CA1a cells (Barbara Ann Karmanos Cancer Institute), and SUM159PT cells (BioIVT) were free of mycoplasma. All cell culture and time-lapse imaging was performed at 37°C and 5% CO_2.

Cell migration studies

For 3D migration assessment, MDA-MB-231 cells were seeded sparsely within 1.5 mg/mL collagen matrices and 3 mg/mL collagen microtracks prepared from acid-solubilized type I rat tail tendon collagen as previously described (14,15).

Phenotypic cell sorting

To purify differentially migratory cells, parental MDA-MB-231 cells (MDA^{PAR}) were seeded in a transwell migration assay. Briefly, a thin 1 mg/mL collagen gel (~10 μm thickness) was polymerized in an 8-μm pore transwell insert (Corning) for 20 min and the coated insert was equilibrated in serum-free DMEM. Cells were plated at 40,000 cells/cm^2 on the gel surface in DMEM + 0.5% FBS, and the insert was placed in a 6 well plate containing DMEM + 10% FBS. On day 2 of culture, the media in the upper reservoir was refreshed. On day 4 of culture, media was removed from both the transwell insert and well plate and reserved. Transwell inserts were washed twice with PBS then 0.25% Trypsin-EDTA was added and the transwell plate was incubated on an orbital shaker at 37ºC for 5 min. The well plate was then removed and tapped gently to help loosen cells then placed back on the orbital shaker for another 5 min. Equal volume of complete media was added above and below the transwell, then cell suspensions were pooled with their respective reserved media. Highly migratory (MDA^+) and weakly migratory (MDA^-) cell subpopulations were recovered by centrifugation from the lower and upper compartment solutions, respectively. Purifying cell sorting was achieved by repeatedly seeding MDA^+ and MDA^- cells on separate freshly prepared transwell migration assays as described above. For purification of MDA^+ cells, cells that migrated through the transwell were recovered and reseeded; for purification of MDA^- cells, cells that did not migrate through the transwell were recovered and reseeded. Twenty rounds of purification were performed. Subpopulations were used in experiments for up to 20 passages following purification with no discernible changes in behavior.

Mice

Experiments were performed in accordance with AAALAC guidelines and were approved by the Vanderbilt University Institutional Animal Care and Use Committee (Protocol#: M1700029–00). 6–8 week old female NOD/SCID immunodeficient mice (The Jackson Laboratory) were injected with 1×10^6 MDA^+ or MDA^- cells subcutaneously at the

mammary gland. Bioluminescence imaging (BLI) was performed using an IVIS™ Spectrum system (PerkinElmer). 150 mg/kg D-luciferin (Gold Biotechnology) was injected intraperitoneally 10 min before imaging. Mice were imaged weekly or biweekly for 4 weeks or until primary tumors approached 100–200 mm^3 in volume. Primary tumor removal surgery followed sterile surgical techniques. After tumor removal, mice were monitored for 4 weeks using BLI. All tissue samples collected were fixed using 4% paraformaldehyde and then processed for histological analysis.

For en bloc tumor collection, mice were injected subcutaneously, and at 4 weeks, the tissue encompassing the primary tumor with an approximately 0.5–1 cm circumferential margin including the overlying skin and the underlying peritoneum was removed such that the surrounding stroma was undisturbed. For circulating tumor cell isolation, mice were injected subcutaneously as described above, and at 4 weeks, blood was obtained via cardiac puncture. The buffy coat was extracted and plated in serum-free DMEM before fixation with 4% paraformaldehyde. For lung decellularization, lungs from FVB mice were collected, processed, and seeded as previously described (16).

Patient blood sample isolation

Cancer patient blood was obtained from patients with stage IV cancer from Guthrie Corning Hospital, after written informed consent (IRB#1402–17). Studies were approved by Institutional Review Boards of Cornell University and Vanderbilt University and were conducted in accordance with the Declaration of Helsinki principles. Samples were shipped overnight and processed as described previously (17,18). Patient outcomes were monitored post-collection for up to 2 years.

For additional information including experimental quantification and statistical analysis, see Supplemental Methods.

Results

Sorting metastatic cancer cells based on migration ability to produce distinct, stable subpopulations

MDA-MB-231 human breast cancer cells are known to be genetically and phenotypically heterogeneous (19,20). To characterize the heterogeneity of their migration phenotype, we seeded MDA-MB-231 cells in 3D collagen matrices and performed time-lapse phase microscopy. The fraction of motile cells increased with time and plateaued at approximately 0.65, indicating that not all cells actively migrate (Fig. 1a). Of those that migrate, some cells displace much more than others (Fig. 1b). A wide distribution of net and total displacements exists (Fig. 1c). To determine whether the migration behavior is heritable, and therefore has the potential to be the basis for phenotypic sorting, the speed of cells prior to and after cell division was measured. Our data indicate that the mother and daughter cell speeds are correlated (Fig. 1d, R^2=0.62), suggesting that migration behavior is heritable.

To sort MDA-MB-231 cells based on migratory ability, MDA-MB-231 (MDA^{PAR}) cells were seeded in low-serum media on top of a collagen-coated transwell with complete media in the bottom chamber. After 4 days, the cells that migrated through the collagen and to

the bottom of the transwell were collected separately from the cells that remained on the top. Both groups were subsequently separately reseeded in fresh transwells, and this sorting process was repeated for 20 rounds to produce stable strongly migratory (MDA^+) and weakly migratory (MDA^-) subpopulations (Fig. 1e). After 20 rounds of sorting, MDA^+ cells were significantly more migratory than MDA^{PAR}, which were significantly more migratory than MDA^- (Fig. 1f). This trend persisted with no significant difference for either subpopulation between their respective freshly sorted cells, cells seeded after a freeze-thaw cycle, and cells that underwent a freeze-thaw cycle followed by subsequent passaging. This indicates the establishment of two stable cell subpopulations that differ in their migration phenotype.

The sorting process requires cells to migrate through collagen. To assess the robustness of the migratory phenotypes and to address the possibility that the response is collagen-specific, we tested the migration behavior of both MDA-MB-231 cell subpopulations in several different matrix compositions and densities. In transwells of increasing collagen density, more migration was observed in MDA^+ compared to MDA^- even as both subpopulations showed decreased fractions of cells migrated with increasing collagen density (Supplementary Fig. 1a). In transwells containing collagen doped with either fibronectin or matrigel, no discernable effect on fractions of cells migrated in either subpopulation was observed with increasing fibronectin or Matrigel concentrations (Supplementary Figs. 1b,c). These results demonstrate that MDA^+ and MDA^- subpopulations retain their migration phenotypes across various ECM compositions and densities.

When seeded in 3D collagen matrix, MDA^+ motile fraction was significantly higher than both MDA^{PAR} and MDA^- motile fractions with MDA^- being significantly lower than MDA^{PAR} (Fig. 1g). MDA^+ cells displaced readily while MDA^- remained largely stationary, toggling in place (Fig. 1h and Supplementary movies 1,2). MDA^+ cells exhibited 3D migration speeds comparable to MDA^{PAR}, which were both significantly higher than MDA^- migration speed (Fig. 1i). These findings suggest that sorting is selecting the most migratory (MDA^+) and least migratory (MDA^-) cells from the parental MDA-MB-231 (MDA^{PAR}) population.

Weakly migratory subpopulation exhibits increased metastatic potential and CTC clustering compared to highly migratory subpopulation

After observing a robust difference in migratory abilities between MDA^+ and MDA^- cells, we next sought to assess their metastatic potentials. Since the acquisition of a migratory phenotype is associated with dissemination from the primary tumor and is often considered essential for metastasis (21,22), we hypothesized that MDA^+ cells would metastasize to a greater extent than MDA^- cells. When cancer cell subpopulations were injected orthotopically into immunocompromised mice, both subpopulations formed primary tumors that grew steadily over the course of four weeks (Fig. 2a). There was no significant difference in primary tumor size upon removal (Fig. 2b). Additionally, subpopulation cell proliferation was compared both in vitro and in vivo and found to be similar (Supplementary Figs. 2a,b). After primary tumor removal, mice were monitored for bioluminescence

signal indicating metastatic spread. Counter to our hypothesis, distal metastatic spread was observed in all MDA^- mice while minimal distal signal was observed in MDA^+ mice (Fig. 2c). These findings were confirmed using anti-GFP immunohistochemistry (IHC) staining of lung, liver, and bone. Extensive metastatic spread was noted in lung, liver, and bone in MDA^- -injected mice while only rarely were micrometastases observed in MDA^+ injected mice (Fig. 2d). Metastatic nodules were observed in MDA^- livers while MDA^+ livers appear healthy (Fig. 2e). Quantification of IHC staining of tissue sections indicates the presence of significantly more GFP-positive cells in MDA^- livers compared to MDA^+ livers (Fig. 2f). In addition, MDA^- livers had significantly more metastatic nodules than MDA^+ livers (Fig. 2g). IHC staining of lung tissue sections were also quantified for GFP-positive cells, and MDA^- lungs had significantly more metastatic colonization than MDA^+ lungs (Figs. 2h,i). To determine whether the weakly migratory phenotype of MDA^- cells that metastasized was preserved, lungs from mice injected orthotopically with MDA^- cells were dissociated and GFP-tagged MDA^- cells were collected via fluorescence activated cell sorting. When seeded in 1.5 mg/mL collagen matrix, metastasized MDA^- cells retained their weakly motile behavior ex vivo (Fig. 2j). Due to the very few metastases that formed in mice injected with MDA^+ cells, we were unable to collect a sufficient number of GFP-positive cells from MDA^+ lungs to make a comparison.

Since this finding that MDA^- are highly metastatic and MDA^+ are poorly metastatic contradicted the prevailing view that robust migration leads to metastasis, we sought to determine whether this finding was specific to MDA-MB-231 cells or whether it also occurs in other cells. MCF10CA1a cells, another metastatic breast cancer cell line, was sorted as before to obtain highly migratory ($CA1a^+$) and weakly migratory ($CA1a^-$) subpopulations (Supplementary Fig. 3a). Upon in vitro seeding in 3D collagen, motile fractions were similar to the behavior of the sorted MDA-MB-231 subpopulations (Supplementary Fig. 3b). Similarly, $CA1a^-$-injected mice exhibited metastasis to lung and lymph nodes to a greater extent than $CA1a^+$-injected mice (Supplementary Fig. 3c,d). SUM159 cells were also sorted to obtain highly migratory ($SUM159^+$) and weakly migratory ($SUM159^-$) subpopulations which exhibited similar differences in motile fraction consistent with the other subpopulations (Supplementary Figs. 4a,b). As observed with the MDA-MB-231 and MCF10CA1a subpopulations, the SUM159—injected mice saw distal metastasis to lung and lymph node that was absent in $SUM159^+$-injected mice (Supplementary Figs. 4c,d). These findings confirmed that the anti-correlation between migration and metastasis was not cell-type specific.

Since MDA^- successfully metastasize whereas MDA^+ do not, we sought to determine at which stage of the metastatic cascade the phenotypically sorted subpopulations differ (Fig. 2k). To assess each subpopulation's ability to migrate locally from the primary tumor, en bloc sections were collected. Based on GFP signal, both subpopulations migrated into stroma adjacent to the primary tumor (Fig. 2l). Quantification of each subpopulation's outgrowth index revealed that both subpopulations migrate locally from the primary tumor; however, MDA^+ cells migrate to a significantly greater extent compared to MDA^- cells (Fig. 2m), as expected based on their in vitro behavior.

We tested whether both subpopulations could successfully intravasate and survive in the circulation. Blood was collected from mice at 4 weeks after tumor induction and circulating tumor cells (CTCs) were isolated and stained for EpCAM and CD45. $GFP^+EpCAM^+CD45^-$ cells were considered CTCs, which were present in blood at similar, high concentrations for both subpopulations (Fig. 2n). However, MDA^- CTCs were present in clusters as well as single cells while MDA^+ CTCs presented as single cell CTCs exclusively (Fig. 2o). To ensure CTCs were being correctly identified, blood from a mouse without cancer cell injections was collected and processed alongside experimental samples, and no CTC-like cells were detected (Supplementary Fig. 5a,b,c). Once CTCs either roll and then attach to the endothelium or lodge in capillary beds, they extravasate out of the circulation (5). To assess extravasation ability, we added the subpopulations to a collagen-coated transwell seeded with an endothelial monolayer. The monolayer was validated using a permeability assay (Supplementary Fig. 5d). After 4 days, both subpopulations migrated into the bottom chamber, although the MDA^+ cells did so significantly more (Fig. 2p). To assess colonization ability, lung tissue was collected from mice, decellularized, and re-seeded with the subpopulations of MDA-MB-231 cells (Supplementary Figs. 5e,f). After 9 days of culture, both subpopulations successfully colonized the decellularized lung ECM (Fig. 2q) to similar extents (Fig. 2r).

Together, these data indicate that despite differences in their migration behaviors, both subpopulations can perform key steps of the metastatic cascade. To further investigate the mechanism by which MDA^- successfully form metastases and MDA^+ do not, we focused on the presence of CTC clusters in MDA^- injected mouse blood, also known as circulating tumor microemboli (CTM), as a potential differentiating factor between the subpopulations which could explain the enhanced metastatic potential of the MDA^- subpopulation.

Phenotypically sorted subpopulations exhibit differential EMT gene regulation

Given these initially counter-intuitive findings that more highly migratory cells are less metastatic and weakly migratory cells are highly metastatic, we sought to investigate the genotypic differences between our phenotypically sorted subpopulations using RNAseq. Initial analysis of sequencing data between MDA^+ and MDA^- subpopulations indicates a large degree of differential gene expression as indicated by the z score heat map (Fig. 3a). As GO term analysis showed biological adhesion and cell motility categories were highly differentially regulated between the subpopulations (Supplementary Table 1), we hypothesized that differential regulation of genes involved in epithelial-to-mesenchymal transition (EMT) could explain the phenotypic differences between our subpopulations. Using a previously published list of genes involved in identification of EMT states (23), a z score heat map comparing epithelial and mesenchymal gene regulation between MDA^+ and MDA^- subpopulations was generated (Supplementary Fig. 6a). We also compared the regulation of these genes between the subpopulations using log 2 fold change (Fig. 3b). In both of these assessments, MDA^+ cells showed greater upregulation of mesenchymal genes while MDA^- cells showed greater upregulation of epithelial genes. MDA^+ cells had both a significantly increased mesenchymal score and decreased epithelial score while MDA^- cells showed the opposite relationship (Figs. 3c,d).

Additionally, we performed RNAseq on the MCF10CA1a subpopulations and found the same trends with a high degree of differential regulation both overall and for EMT genes (Supplementary Figs. 7a,b,c). The $CA1a^+$ subpopulation showed significant upregulation of mesenchymal scores and downregulation of epithelial scores while the $CA1a^-$ subpopulation showed the opposite trends (Supplementary Figs. 7d,e). These same trends in overall expression and EMT gene regulation followed for the SUM159 subpopulations where the $SUM159^+$ subpopulation showed enhanced mesenchymal and reduced epithelial scores and the $SUM159^-$ subpopulation showed the converse (Supplementary Figs. 8a,b,c,d,e). When GO term analysis on these sets of subpopulations were performed, both showed biological adhesions as one of the most differentially regulated GO term categories (Supplementary Table 1). Given the consistency of this finding across cell lines and the CTC clustering observed in MDA—injected mice, we hypothesized that cell-cell adhesion may be involved in the differential metastatic phenotype. To further characterize cell-cell adhesion behavior across all subpopulations, RNAseq data for genes encoding cell-cell adhesion proteins were compared, and cell-cell adhesion scores were calculated. Weakly migratory subpopulations from MDA-MB-231 (Supplementary Figs. 9a,b,c), MCF10CA1a (Supplementary Figs. 10a,b,c), and SUM159 (Supplementary Figs. 11a,b,c) cell lines showed a significantly higher cell-cell adhesion score than their respective highly migratory subpopulations, indicating greater upregulation of cell-cell adhesion genes. Interestingly, E-cadherin, a cell-cell adhesion protein that has been recently implicated in CTC clustering and metastatic potential in other systems (24,25), was the most highly differentially upregulated epithelial marker in MDA^- cells compared to MDA^+ cells.

E-cadherin expression in phenotypically sorted subpopulations is necessary for successful completion of the metastatic cascade

Based on the formation of MDA^- CTM in the circulation and our RNAseq data, we investigated the role of E-cadherin, a cell-cell adhesion protein implicated in CTM formation (26–28). MDA^- cells were found to possess significantly higher E-cadherin compared to MDA^+ based on both qPCR (Fig. 4a) and western blotting (Fig. 4b, Supplementary Fig. 12a). Immunofluorescence staining for E-cadherin in MDA^- cells indicated that it is localized to cell-cell junctions within cell clusters (Fig. 4c). These assays confirm that MDA^- cells express E-cadherin.

To determine whether E-cadherin expression was involved in the increased metastatic potential of MDA^- cells, an E-cadherin knockdown cell line was created by transducing MDA^- cells with E-cadherin shRNA (Supplementary Fig. 12b). When E-cadherin knockdown MDA^- (EcadKD) cells were injected orthotopically, BLI signal indicated slightly slowed growth of EcadKD primary tumors compared to MDA^- scrambled shRNA control (Scrambled) primary tumors (Fig. 4d). To compensate for this, EcadKD primary tumors were removed after they reached a comparable size to control tumors. After primary tumor removal, BLI showed reduced distal metastasis in EcadKD mice compared to control mice (Fig. 4e). Anti-GFP IHC staining of lungs and liver confirmed a marked decrease in distal metastasis in EcadKD mice compared to scrambled control mice (Fig. 4f). Additionally, macroscopically, there were significantly fewer liver nodules in EcadKD compared to controls (Supplementary Fig. 12c). When quantified, a significantly greater

percentage of GFP-positive cells were found in liver (Fig. 4g) and lungs (Fig. 4h) of scrambled control mice compared to EcadKD. These findings suggest that E-cadherin promotes distal metastasis of the MDA^- subpopulation and may be required for metastasis of these cells.

To determine whether E-cadherin expression can enable the MDA^+ subpopulation to metastasize, we transduced MDA^+ cells to express E-cadherin (Fig. 4i, Supplementary Fig. 12d). Primary tumor growth was monitored using BLI, and primary tumors were removed at 4 weeks (Fig. 4j). At the study endpoint, distal metastasis can be consistently observed in MDA^+ + E-cadherin injected mice via BLI in locations indicative of lungs, liver, and bone (Fig. 4k). Metastasis to lungs and liver was confirmed using anti-GFP IHC staining (Fig. 4l). Additionally, quantification of metastatic liver nodules reveals a significantly higher nodule count for MDA^+ + E-cadherin mice compared to MDA^+ mice (Supplementary Fig. 12e). When quantified, the percentage of GFP-positive cells was significantly higher in liver (Fig. 4m) and lungs (Fig. 4n) of MDA^+ + E-cadherin mice compared to MDA^+ mice. At 4 weeks post-injection, CTCs were collected from MDA^-EcadKD- and MDA^+ + E-cadherin-injected mice as before, and no significant difference in CTC concentration for these conditions compared to either MDA^+- or MDA^--injected mice was observed (Supplementary Fig. 12f). Further, CTC clusters were abrogated in MDA^-EcadKD-injected mice while CTC clusters were present in MDA^+ + E-cadherin-injected mice (Supplementary Fig. 12g). Together, these results establish that E-cadherin expression enables successful distal metastasis in both of our phenotypically sorted subpopulations and that E-cadherin plays a role in CTC clustering.

E-cadherin expression tunes migration mode and extent in subpopulations

Our data indicate that E-cadherin expression is related to the metastatic phenotype of highly migratory MDA^+ and weakly migratory MDA^- cell subpopulations. However, the molecular mechanism governing their difference in migration behavior in vitro is not clear. To determine whether E-cadherin plays a role in migration phenotype, we sought to further characterize these subpopulations and their variants to determine if modulation of E-cadherin expression would be sufficient to affect their distinct migratory phenotypes in vitro.

First, we characterized the localization of E-cadherin across all MDA-MB-231 conditions (Supplementary Fig. 13a). As seen in the representative immunofluorescence images, as expected, E-cadherin localizes to junctions as well as the cytoplasm in cells within MDA^-, MDA^+Ecad^{Low} (used for in vivo experiments described above), and MDA^+Ecad^{High} (transduced with comparatively much higher E-cadherin expression) subpopulations while it is observed cytoplasmically in cells within the MDA^{PAR} population and is absent from MDA^+ and MDA^-EcadKD cells. We revisited the transwell migration sorting platform to determine if modulation of E-cadherin expression affects either subpopulation's ability to migrate through a collagen-coated transwell membrane. As expected, MDA^+ cells migrated through the transwell significantly more than MDA^{PAR}, which migrated significantly more than MDA^- (Fig. 5a). When MDA^+ cells were induced to express a relatively modest amount of E-cadherin that was used previously in our in vivo experiments (MDA^+Ecad^{Low}),

the fraction of cells migrated significantly decreased, whereas when E-cadherin was knocked down in MDA^- cells, the fraction of cells migrated significantly increased. However, even with a much higher level of E-cadherin expression, MDA^+Ecad^{High} cells still migrated significantly more than MDA^- cells. The migration fraction for MDA^+Ecad^{Low} cells was significantly higher than MDA^-EcadKD cells indicating that E-cadherin alone is not responsible for the differences in migration ability. We also compared the motile fraction of each condition seeded as single cells in 3D collagen matrix (Fig. 5b). Here, we found similar trends where E-cadherin addition significantly attenuated the motile fractions of both MDA^+Ecad^{Low} and MDA^+Ecad^{High} conditions compared to MDA^+, and knockdown significantly enhanced the motile fraction of MDA^-EcadKD cells compared to MDA^- cells. Here, even the much higher level of E-cadherin expression in MDA^+Ecad^{High} was not sufficient to lower motile fraction to MDA^- or MDA^-EcadKD levels. These data show that E-cadherin affects the migration of the phenotypically sorted subpopulations but does not completely explain their distinct migratory abilities.

Given that MDA^- are relatively weak migrators, we sought to determine whether their migration defect was related to their ability to remodel matrix to facilitate movement. It has been previously shown that cancer cells can utilize channels found in native mammary stroma to migrate independent of proteolysis and matrix reorganization (8). To test whether MDA^- are capable of migrating in the more permissive environment of collagen channels, subpopulations were seeded in channels micromolded into collagen, and phase time-lapse microscopy was performed. MDA^+ cells in channels displaced more readily than MDA^- cells in channels (Supplementary movies 3,4), indicating that this permissive environment is not sufficient to improve MDA^- migration ability to levels comparable to MDA^+. Cell velocities in the channels were quantified and MDA^+ cells migrated significantly faster than MDA^{PAR} cells, which migrated significantly faster than MDA^- cells (Fig. 5c). In the channels, MDA^+Ecad^{Low} and MDA^+Ecad^{High} cell velocities were not significantly different from that of MDA^-EcadKD cells. This suggests that while there are still additional factors responsible for part of the differential migration modes of these subpopulations, decreased ability to remodel matrix could also contribute to a portion of the residual differences that remain between the subpopulations after E-cadherin is altered.

While single cell migration models are often used to study cancer cell migration, collective migration is thought to be the more prevalent mode of migration in vivo (29). To assess the migration ability of these subpopulations and their E-cadherin variants in a collective context, in vitro tumor spheroids were formed. When embedded in collagen and monitored for 48 h, all conditions resulted in spheroid outgrowth into the surrounding matrix (Fig. 5d). MDA^- spheroids outgrew significantly less than MDA^{PAR}, which outgrew significantly less than MDA^+ spheroids (Fig. 5e). Consistent with single cell measurements, outgrowth area of MDA^+Ecad^{Low} and MDA^+Ecad^{High} spheroids were significantly reduced compared to MDA^+ spheroids, and outgrowth area significantly increased in MDA^-EcadKD spheroids compared to MDA^- control spheroids. Interestingly, MDA^+ spheroids migrated out largely as single cells while MDA^- spheroids migrated as collective strands while MDA^{PAR} spheroids presented as a mixture of the two modes. This suggests that while MDA^- cells do not migrate well as single cells, they are able to migrate collectively albeit less effectively than MDA^+ cells. Additionally, while MDA^+Ecad^{Low} spheroids exhibit reduced outgrowth

but no noticeable change in migration mode compared to MDA^+ spheroids, MDA^+Ecad^{High} spheroids shift from single to collective migration modes and obtain a reduced outgrowth area similar to that of MDA^- spheroids. Conversely, MDA^-EcadKD spheroids retain the collective mode of migration while exhibiting a higher outgrowth area compared to MDA^- spheroids. Together, this suggests that while E-cadherin expression can modulate cell migration in both single and collective contexts, there are still other inherent differences between these subpopulations that affect their determining migration ability.

Phenotypically sorted subpopulations display different morphologies and contractility

After further characterizing the migration abilities of phenotypically sorted weakly and highly migratory cells and their E-cadherin variants, we sought to examine cytoskeletal architecture, cell-ECM signaling, and mechanotransduction, since these all can impact migration ability. To assess the morphologies of the phenotypically sorted cells with and without E-cadherin, we imaged them using phase-contrast microscopy (Fig. 6a). The MDA^+ and MDA^- display distinct phenotypes which are present in the heterogeneous parental cells. When comparing the morphologies of MDA^+, MDA^+Ecad^{Low}, and MDA^+Ecad^{High}, more cell spreading and cell-cell contacts occur as E-cadherin expression increases. Conversely, when comparing the MDA^- and MDA^-EcadKD cell morphologies, there is a slight reduction in cell-cell contacts and cell spreading. When cell area is quantified, MDA^- cells have significantly greater cell area compared to MDA^{PAR} cells which have greater cell area than MDA^+ cells (Fig. 6b). Interestingly, both the addition or knockdown of E-cadherin to MDA^+ and MDA^- cells, respectively, result in increased cell area compared to the baseline phenotypes.

Since migration behavior is dependent on cytoskeletal architecture (11), actin staining was performed on both subpopulations. MDA^- cells exhibit robust stress fibers while MDA^+ cells display both stress fibers as well as ruffling lamellipodia (Supplementary Fig. 14a). Again, MDA^{PAR} cells display attributes of both subpopulations and E-cadherin addition or knockdown can attenuate these phenotypes in each respective subpopulation. Lamellipodia formation has been associated with both migratory and metastatic phenotypes (30). Additionally, stress fibers in non-motile cells are expected to be more robust compared to stress fibers in migratory cells (31). Thus, the prevalence of lamellipodia in MDA^+ and stress fibers in MDA^- are consistent with their migratory phenotypes. Together, these data show that the subpopulations display distinct morphologies that are present in the heterogeneous parental population and can be altered by changing E-cadherin expression.

Since the actin cytoskeleton and cell-matrix adhesions are interdependent (32), we examined adhesive structures and signaling across all cell conditions. Since focal adhesion kinase (FAK) has been correlated with an invasive phenotype and metastasis (33), we investigated whether subpopulations had differential FAK expression and activation. While total FAK levels were similar between subpopulations, MDA^- cells had significantly higher FAK activation compared to MDA^+ as indicated by pFAK/FAK levels (Figs. 6c,f). Western blotting shows that loss of E-cadherin in MDA^- reduces FAK activation (Figs. 6d,g) while addition of E-cadherin to MDA^+ increases FAK activation (Figs. 6e,h). To further characterize focal adhesions, we performed staining for phosphorylated FAK, which

revealed small, nascent focal adhesions localized at the lamellipodium in MDA^+ cells and large, elongated focal adhesions capping stress fibers in MDA^- (Supplementary Fig. 14a). When quantified, MDA^- cells had significantly larger focal adhesions than MDA^{PAR}, which had larger focal adhesions than MDA^+ (Fig. 6i). When E-cadherin was knocked out in MDA^-, focal adhesion area decreased while when E-cadherin was added to MDA^+ cells, it was increased. Together, these results suggest that MDA^+ and MDA^- subpopulations have differential FAK signaling which is mediated in part by E-cadherin.

Given the robust differences in morphologies and cytoskeletal architecture between the subpopulations, traction force microscopy (TFM) was performed to quantify contractile forces generated by MDA^+ and MDA^- cells with and without E-cadherin. Prior work indicates traction stresses are increased in malignant and more metastatic cells (34,35). While both subpopulations were not significantly different from MDA^{PAR}, traction forces of MDA^+ were significantly increased compared to MDA^- (Fig. 6j). To determine whether this trend persists in 3D collagen matrix, a collagen contraction assay was performed. MDA^+ seeded collagen gels contracted significantly more than MDA^{PAR} seeded collagen gels which contracted more than MDA^- seeded collagen gels (Fig. 6k). These data indicate that the highly motile, weakly metastatic subpopulation is more contractile than the weakly motile, highly metastatic subpopulation, which is counter to the hypothesis that more malignant and metastatic cells exert higher forces (34,35). While MDA^+Ecad^{High} exhibited relatively weak traction stresses in the TFM assay, this condition showed compaction comparable to those of MDA^+ gels in the collagen gel contraction assay (Fig. 6j,k). In addition, in vitro tumor spheroids were imaged at 24 h post-embedding using quantitative polarization microscopy to assess cell contractility in the context of multicellular cancer cell strand migration (Supplementary Fig. 15a). Here, optical anisotropy (which represents the contractility of cells within the migration strands) of each condition shows comparable trends to the TFM and gel contraction assay data. The optical anisotropy signal is highest in MDA^+ migrating cells compared to MDA^{PAR} cells which show higher optical anisotropy signal than cells in MDA^- migration strands. Additionally, MDA^+Ecad^{Low} migrating cells have lower optical anisotropy signal compared to MDA^+ cells but greater signal than cells in MDA^+Ecad^{High} migration strands. MDA^-EcadKD migration strands showed higher optical anisotropy signal compared to MDA^- migration strands.

Together, this data demonstrates that phenotypically sorted subpopulations possess unique cytoskeletal features, cell-ECM signaling, and contractility behavior that are distinct even when modulated by E-cadherin expression.

Clustering of circulating tumor cells in patient blood correlates with prognosis

Based on our data, the MDA^- subpopulation has a higher metastatic fitness that is associated with E-cadherin expression and clustering of CTCs. To determine if CTC clustering and E-cadherin expression are clinically relevant markers of metastatic potential, blood samples from patients with metastatic cancer were collected and processed (Supplementary Table 2). After staining for cytokeratin, single CTCs and CTC clusters were quantified (Fig. 7a). Our data indicate there is a significant trend between the concentration of CTC clusters per mL blood and patient survival, where patients with survival time of less than 12 months

had significantly increased CTC cluster concentrations compared to patients with 12–24 month survival and those alive with progression (Fig. 7b). In a separate cohort of metastatic breast cancer patient samples (Supplementary Table 3), when stained for E-cadherin, both single cell and clustered CTCs in metastatic breast cancer patient blood were positive for E-cadherin in all patient samples tested (Fig. 7c). Additionally, we used a Kaplan-Meier Plotter to determine the relationship between E-cadherin and distal metastasis-free survival (DMFS) and overall survival (OS) in breast cancer patients (36). The upper tercile of patients based on E-cadherin gene expression showed a significant reduction in both DMFS (Fig. 7d) and OS (Fig. 7e) compared to the lower tercile of patients. These results suggest E-cadherin expression and CTC clustering have prognostic value in breast cancer.

Discussion

Here, we used the approach of sorting cells based on migratory phenotype to identify the phenotype associated with the most aggressively metastatic cells. MDA^+ and MDA^- subpopulations were sorted based on their ability to migrate through a transwell migration assay. Notably, MDA^- cells were highly metastatic in vivo compared to MDA^+ cells when injected orthotopically into mice. RNA sequencing revealed robust differences in gene regulation across many aspects of cellular function including cell adhesion and motility, which are associated with epithelial-to-mesenchymal transition (EMT). MDA^- cells showed increased epithelial gene expression compared to MDA^+ cells, which showed increased mesenchymal gene expression. The increased metastatic potential of MDA^- was found to be dependent on E-cadherin, which enabled CTC clusters to form and disseminate in the circulation leading to enhanced colonization of distant tissues. Further, we established that induced expression of E-cadherin was sufficient to rescue MDA^+ cells and allow them to metastasize to the same tissues as MDA^-. Notably, in cancer patients, the number of CTC clusters in blood trended with worsened patient outcomes, CTCs from metastatic breast cancer patients were found to be positive for E-cadherin, and E-cadherin was associated with decreased distal metastasis free survival and overall survival. Together, these data indicate that migration ability in vitro is not positively correlated with metastasis, and E-cadherin plays a significant role in determining metastasis.

Perhaps one of the most surprising results from this study is that migration ability does not correlate with metastasis. Our results generate numerous questions regarding intratumor heterogeneity in the context of migratory and metastatic phenotypes. Importantly, how much value should be placed on single cell migration studies and the most migratory cells in a population in cancer research? Even in highly permissive collagen microtracks, MDA^- cells migrated poorly until placed in the collective context of in vitro tumor spheroids. Given that our MDA^- subpopulation migrates poorly as single cells compared to in spheroids when they are permitted to migrate collectively, many researchers focused on single cell assays might inadvertently dismiss these cells, as motility is often correlated with cancer aggressiveness. Thus, these results highlight the need for physiologically relevant multicellular migration assays that can allow more complex cell behaviors, such as collective migration to be observed. Even with that consideration, our data indicate that migration ability, even when in a collective context, is not predictive of metastasis.

Based on our findings, E-cadherin, an epithelial protein that is generally considered a tumor suppressor, enables breast cancer metastasis. Epithelial-to-mesenchymal transition (EMT) has traditionally been considered necessary for metastasis, with cancer aggressiveness and metastatic potential correlating with the extent of EMT (37,38). Increasing evidence calls into question the necessity of traditionally defined EMT and places increasing importance on cells that possess the capacity to exhibit epithelial properties required for metastatic colonization (38–40). E-cadherin along with other epithelial markers including keratin-14 have been shown to facilitate metastasis (40,41). The enabling role of E-cadherin for metastasis and reciprocal effects on migration were recently delineated in several breast cancer models (24,25). Our data may suggest that E-cadherin expression in the MDA^- subpopulation endows these cells with a hybrid epithelial/mesenchymal (E/M) phenotype, which has been suggested to enhance metastatic potential (42–45). The MDA^+ subpopulation may represent an extreme mesenchymal phenotype, which lacks the epithelial traits necessary for metastatic colonization (38,42,46,47). Probing the effects on both migration and metastasis of other epithelial and mesenchymal genes that we assessed using RNA sequencing could help determine which are associated with hybrid or extreme EMT states. As intermediate EMT states are being characterized, further work should be done towards probing heterogeneity of the EMT spectrum within primary tumors and metastatic sites.

We have shown that MDA^- are capable of migrating collectively in an in vitro tumor spheroid model but do not know what specific cues and machinery enable this migration. In Drosophila, E-cadherin has been shown to play a critical role as a mechanical signal integrator where it was necessary for directed migration of cellular clusters (48). Using MDCK cells, it was recently shown that FAK-Src signaling is involved in relaxation of E-cadherin tension which facilitates migration via β-catenin signaling (49). Given our findings that MDA^- cells exhibited higher FAK activation compared to MDA^+ cells, further work should be done to determine if FAK signaling plays a role in the collective migration abilities of MDA^-. E-cadherin loss in MDA^- cells increased migration, consistent with findings of others (24,50), but was not sufficient to completely alter migration mode, indicating that there are other factors, most likely other epithelial cell-cell adhesion proteins, contributing to this behavior.

One caveat of this study is that the implications of our phenotypic cell sorting process on the resulting subpopulations remain incompletely understood. One limitation of the transwell sorting platform is that it does not lend itself to real-time observation, which could provide more insight into the migration modes of the subpopulations when migrating through the transwell membrane. While none of the behaviors observed in either subpopulations appear to reside outside of the range of MDA^{PAR} behaviors, it remains possible that the 20 rounds of sorting could condition or evolve the cells in a way that we have not yet identified. While this assay's greatest perceived strength is that instead of selecting for protein expression or another well-defined metric, we are selecting for the multi-faceted behavior of cell migration, it is important to note that this limits our understanding of how these subpopulations relate to fully heterogeneous, unsorted parental cells. Further efforts to elucidate how representative these subpopulations are in the context of their parental cell lines should be considered as well as continued interrogation of the MCF10CA1a

and SUM159 subpopulations as the notable transcriptional differences observed in the subpopulations across all three triple negative breast cancer cells lines test may contribute novel insight into the mechanisms of migration and metastasis. Additionally, comparison with subpopulations obtained from phenotypic sorting methods based on other cell behaviors such as adhesion and metastatic site preference could provide a more complete understanding of intratumor heterogeneity in the context of metastasis (51–53).

Our data supports the critical role of hybrid E/M phenotypes and the concept that certain subpopulations of cells, in this case MDA^+ cells, can be too mesenchymal, lacking epithelial features required to colonize metastatic sites. We have demonstrated that E-cadherin facilitates cancer metastasis in weakly motile cells and can ameliorate the metastatic potential of highly migratory cells. Since colonization is the step in metastasis in which cancer gains its lethality, future therapeutic strategies could potentially take advantage of these findings by forcing metastatic cancer cells towards an extreme mesenchymal phenotype to prevent colonization and disease progression.

Supplementary Material

Refer to Web version on PubMed Central for supplementary material.

Acknowledgements

This work was performed in part at the Translational Pathology Shared Resource, which is supported by NCI/NIH Cancer Center Support Grant 2P30 CA068485–14 and the Vanderbilt Mouse Metabolic Phenotyping Center Grant 5U24DK059637–13. We would like to thank Dr. Craig Duvall for the use of the IVIS Lumina III, Dr. Thong Cao for plasmid design, and Caroline Carlson for assisting with data analysis.

Financial support: This work was supported by the Keck Foundation, The National Institutes of Health (GM131178) and a National Science Foundation-National Institutes of Health Award (1740900) (to C. A. Reinhart-King), National Science Foundation Graduate Research Fellowship Award under Grant No. DGE-1650441 (to L.A. Hapach, S.P. Carey, M.C. Lampi, and N. Ortiz-Otero) and under Grant No. 1937963 (to S.C. Schwager and J.A. Mosier) and Scholarship for the Next Generation of Scientists from the Cancer Research Society and National Cancer Institute Grant K99CA212270 (to F. Bordeleau).

References:

1. Zardavas D, Irrthum A, Swanton C, Piccart M. Clinical management of breast cancer heterogeneity. Nat Rev Clin Oncol. 2015;12:381–94. [PubMed: 25895611]
2. Yang F, Wang Y, Li Q, Cao L, Sun Z, Jin J, et al. Intratumor heterogeneity predicts metastasis of triplenegative breast cancer. Carcinogenesis. 2017;38:900–9. [PubMed: 28911002]
3. Turajlic S, Swanton C. Metastasis as an evolutionary process. Science. 2016;352:169–75. [PubMed: 27124450]
4. Lin JMG, Kang CC, Zhou Y, Huang H, Herr AE, Kumar S. Linking invasive motility to protein expression in single tumor cells. Lab Chip. 2018;18:371–84. [PubMed: 29299576]
5. Hapach LA, Mosier JA, Wang W, Reinhart-King CA. Engineered models to parse apart the metastatic cascade. npj Precis Oncol 2019;3:20. [PubMed: 31453371]
6. Wu Y, Siadaty MS, Berens ME, Hampton GM, Theodorescu D. Overlapping gene expression profiles of cell migration and tumor invasion in human bladder cancer identify metallothionein 1E and nicotinamide N-methyltransferase as novel regulators of cell migration. Oncogene. 2008;27:6679–89. [PubMed: 18724390]
7. Clark AG, Vignjevic DM. Modes of cancer cell invasion and the role of the microenvironment. Curr Opin Cell Biol. 2015;36:13–22. [PubMed: 26183445]

8. Carey SP, Rahman A, Kraning-Rush CM, Romero B, Somasegar S, Torre OM, et al. Comparative mechanisms of cancer cell migration through 3D matrix and physiological microtracks. Am J Physiol - Cell Physiol. 2015;308:436–47.

9. Riching KM, Cox BL, Salick MR, Pehlke C, Riching AS, Ponik SM, et al. 3D Collagen Alignment Limits Protrusions to Enhance Breast Cancer Cell Persistence. Biophysj. 2014;107:2546–58.

10. Carey SP, Goldblatt ZE, Martin KE, Romero B, Williams RM, Reinhart-King CA. Local extracellular matrix alignment directs cellular protrusion dynamics and migration through Rac1 and FAK. Integr Biol. 2016;8:821–35.

11. Bordeleau F, Alcoser TA, Reinhart-King CA. Physical biology in cancer. 5. The rocky road of metastasis: The role of cytoskeletal mechanics in cell migratory response to 3D matrix topography. Am J Physiol- Cell Physiol. 2014;306:110–20.

12. Schor SL. Cell proliferation and migration on collagen substrata in vitro. J Cell Sci. 1980;41:159–75. [PubMed: 7364880]

13. Aznavoorian S, Murphy AN, Stetler SW, Liotta LA. Molecular aspects of tumor cell invasion and metastasis. Cancer. 1993;71:1368–83. [PubMed: 8435813]

14. Carey SP, Starchenko A, McGregor AL, Reinhart-King CA. Leading malignant cells initiate collective epithelial cell invasion in a three-dimensional heterotypic tumor spheroid model. Clin Exp Metastasis. 2013;30:615–30. [PubMed: 23328900]

15. Kraning-Rush CM, Carey SP, Lampi MC, Reinhart-King CA. Microfabricated collagen tracks facilitate single cell metastatic invasion in 3D. Integr Biol. 2013;5:606–16.

16. Xiong G, Flynn T, Chen J, Trinkle C, Xu R. Development of an ex vivo breast cancer lung colonization model utilizing decellularized lung matrix. Integr Biol. 2015;7:1518–25.

17. Hughes AD, Marshall JR, Keller E, Powderly JD, Greene BT, King MR. Differential drug responses of circulating tumor cells within patient blood. Cancer Lett. 2014;28:28–35.

18. Meye A, Bilkenroth U, Schmidt U, Fussel S, Robel K, Melchior AM, et al. Isolation and enrichment of urologic tumor cells in blood samples by a semi-automated CD45 depletion autoMACS protocol. Int J Oncol. 2002;21:521–30. [PubMed: 12168095]

19. Ali R, Wendt MK. The paradoxical functions of EGFR during breast cancer progression. Signal Transduct Target Ther. 2017;2:1–7.

20. Martín-Pardillos A, Valls Chiva Á, Bande Vargas G, Hurtado Blanco P, Piñeiro Cid R, Guijarro PJ, et al. The role of clonal communication and heterogeneity in breast cancer. BMC Cancer. 2019;19:1–26. [PubMed: 30606139]

21. Koedoot E, Fokkelman M, Rogkoti VM, Smid M, van de Sandt I, de Bont H, et al. Uncovering the signaling landscape controlling breast cancer cell migration identifies novel metastasis driver genes. Nat Commun. 2019;10:1–16. [PubMed: 30602773]

22. Jiang WG, Sanders AJ, Katoh M, Ungefroren H, Gieseler F, Prince M, et al. Tissue invasion and metastasis: Molecular, biological and clinical perspectives. Semin Cancer Biol. 2015;35:244–75.

23. Pastushenko I, Brisebarre A, Sifrim A, Fioramonti M, Revenco T, Boumahdi S, et al. Identification of the tumour transition states occurring during EMT. Nature. 2018;556:463–8. [PubMed: 29670281]

24. Padmanaban V, Krol I, Suhail Y, Szczerba BM, Aceto N, Bader JS, et al. E-cadherin is required for metastasis in multiple models of breast cancer. Nature. Springer US; 2019;324:439–44.

25. Elisha Y, Kalchenko V, Kuznetsov Y, Geiger B. Dual role of E-cadherin in the regulation of invasive collective migration of mammary carcinoma cells. Sci Rep. 2018;8:1–15. [PubMed: 29311619]

26. Aceto N, Bardia A, Miyamoto DT, Donaldson MC, Wittner BS, Spencer JA, et al. Circulating tumor cell clusters are oligoclonal precursors of breast cancer metastasis. Cell. 2014;158:1110–22. [PubMed: 25171411]

27. Giuliano M, Shaikh A, Lo HC, Arpino G, De Placido S, Zhang XH, et al. Perspective on circulating tumor cell clusters: Why it takes a village to metastasize. Cancer Res. 2018;78:845–52. [PubMed: 29437766]

28. Mutlu BR, Dubash T, Dietsche C, Mishra A, Ozbey A, Keim K, et al. In-flow measurement of cell–cell adhesion using oscillatory inertial microfluidics. Lab Chip. 2020;1612–20. [PubMed: 32301448]

29. Lintz M, Muñoz A, Reinhart-King CA. The Mechanics of Single Cell and Collective Migration of Tumor Cells. J Biomech Eng. 2017;139:1–9.
30. Baugher PJ, Krishnamoorthy L, Price JE, Dharmawardhane SF. Rac1 and Rac3 isoform activation is involved in the invasive and metastatic phenotype of human breast cancer cells. Breast Cancer Res. 2005;7:R965–74. [PubMed: 16280046]
31. Tojkander S, Gateva G, Lappalainen P. Actin stress fibers - Assembly, dynamics and biological roles. J Cell Sci. 2012;125:1855–64. [PubMed: 22544950]
32. Huveneers S, Danen EHJ. Adhesion signaling - Crosstalk between integrins, Src and Rho. J Cell Sci. 2009;122:1059–69. [PubMed: 19339545]
33. Luo M, Guan J-L. Focal Adhesion Kinase: a Prominent Determinant in Breast Cancer Initiation, Progression, and Metastasis. Cancer Lett. 2010;289:127–39. [PubMed: 19643531]
34. Paszek MJ, Zahir N, Johnson KR, Lakins JN, Rozenberg GI, Gefen A, et al. Tensional homeostasis and the malignant phenotype. Cancer Cell. 2005;8:241–54. [PubMed: 16169468]
35. Kraning-Rush CM, Califano JP, Reinhart-King CA. Cellular traction stresses increase with increasing metastatic potential. PLoS One. 2012;7.
36. Győrffy B, Lanczky A, Eklund AC, Denkert C, Budczies J, Li Q, et al. An online survival analysis tool to rapidly assess the effect of 22,277 genes on breast cancer prognosis using microarray data of 1,809 patients. Breast Cancer Res Treat. 2010;123:725–31. [PubMed: 20020197]
37. Venhuizen J-H, Jacobs FJC, Span PN, Zegers MM. P120 and E-cadherin: double-edged swords in tumor metastasis. Semin Cancer Biol. 2019;1–14.
38. Wells A, Chao YL, Grahovac J, Wu Q, Lauffenburger DA. Epithelial and mesenchymal phenotypic switchings modulate cell motility in metastasis. Front Biosci. 2011;16:815–37.
39. Fischer KR, Durrans A, Lee S, Sheng J, Li F, Wong STC, et al. Epithelial-to-mesenchymal transition is not required for lung metastasis but contributes to chemoresistance. Nature. 2015;527:472–6. [PubMed: 26560033]
40. Cheung KJ, Gabrielson E, Werb Z, Ewald AJ. Collective invasion in breast cancer requires a conserved basal epithelial program. Cell. 2013;155:1639–51. [PubMed: 24332913]
41. Russo GC, Karl MN, Clark D, Cui J, Carney R, Su B, et al. E-cadherin promotes cell hyper-proliferation in breast cancer. BioRxiv. 2020;
42. Liu X, Li J, Cadilha BL, Markota A, Voigt C, Huang Z, et al. Epithelial-type systemic breast carcinoma cells with a restricted mesenchymal transition are a major source of metastasis. Sci Adv. 2019;5:1–18.
43. Jolly MK, Tripathi SC, Jia D, Mooney SM, Celiktas M, Hanash SM, et al. Stability of the hybrid epithelial/mesenchymal phenotype. Oncotarget. 2016;7:27067–84. [PubMed: 27008704]
44. Lu M, Jolly MK, Levine H, Onuchic JN, Ben-Jacob E. MicroRNA-based regulation of epithelial-hybrid-mesenchymal fate determination. Proc Natl Acad Sci U S A. 2013;110:18144–9. [PubMed: 24154725]
45. Saitoh M. Involvement of partial EMT in cancer progression. J Biochem. 2018;164:257–64. [PubMed: 29726955]
46. Ocaña OH, Córcoles R, Fabra Á, Moreno-Bueno G, Acloque H, Vega S, et al. Metastatic Colonization Requires the Repression of the Epithelial-Mesenchymal Transition Inducer Prrx1. Cancer Cell. 2012;22:709–24. [PubMed: 23201163]
47. Tsai JH, Donaher JL, Murphy DA, Chau S, Yang J. Spatiotemporal Regulation of Epithelial-Mesenchymal Transition Is Essential for Squamous Cell Carcinoma Metastasis. Cancer Cell. 2012;22:725–36. [PubMed: 23201165]
48. Cai D, Chen S, Prasad M, He L, Wang X, Sawyer JK, et al. Mechanical feedback through E-cadherin promotes direction sensing during collective cell migration. 2015;157:1146–59.
49. Gayrard C, Bernaudin C, Déjardin T, Seiler C, Borghi N. Src- and confinement-dependent FAK activation causes E-cadherin relaxation and β-catenin activity. J Cell Biol. 2018;217:1063–77. [PubMed: 29311227]
50. Chao YL, Shepard CR, Wells A. Breast carcinoma cells re-express E-cadherin during mesenchymal to epithelial reverting transition. Mol Cancer. 2010;9:1–18. [PubMed: 20051109]

51. Fuhrmann A, Banisadr A, Beri P, Tlsty TD, Engler AJ. Metastatic State of Cancer Cells May Be Indicated by Adhesion Strength. Biophys J. Biophysical Society; 2017;112:736–45.

52. Beri P, Popravko A, Yeoman B, Kumar A, Chen K, Hodzic E, et al. Cell adhesiveness serves as a biophysical marker for metastatic potential. Cancer Res. 2020;80:901–11. [PubMed: 31857292]

53. Minn AJ, Kang Y, Serganova I, Gupta GP, Giri DD, Doubrovin M, et al. Distinct organ-specific metastatic potential of individual breast cancer cells and primary tumors. J Clin Invest. 2005;115:44–55. [PubMed: 15630443]

Statement of Significance:

This study employs phenotypic cell sorting for migration to reveal a weakly migratory, highly metastatic breast cancer cell subpopulation regulated by E-cadherin, highlighting the dichotomy between cancer cell migration and metastasis.

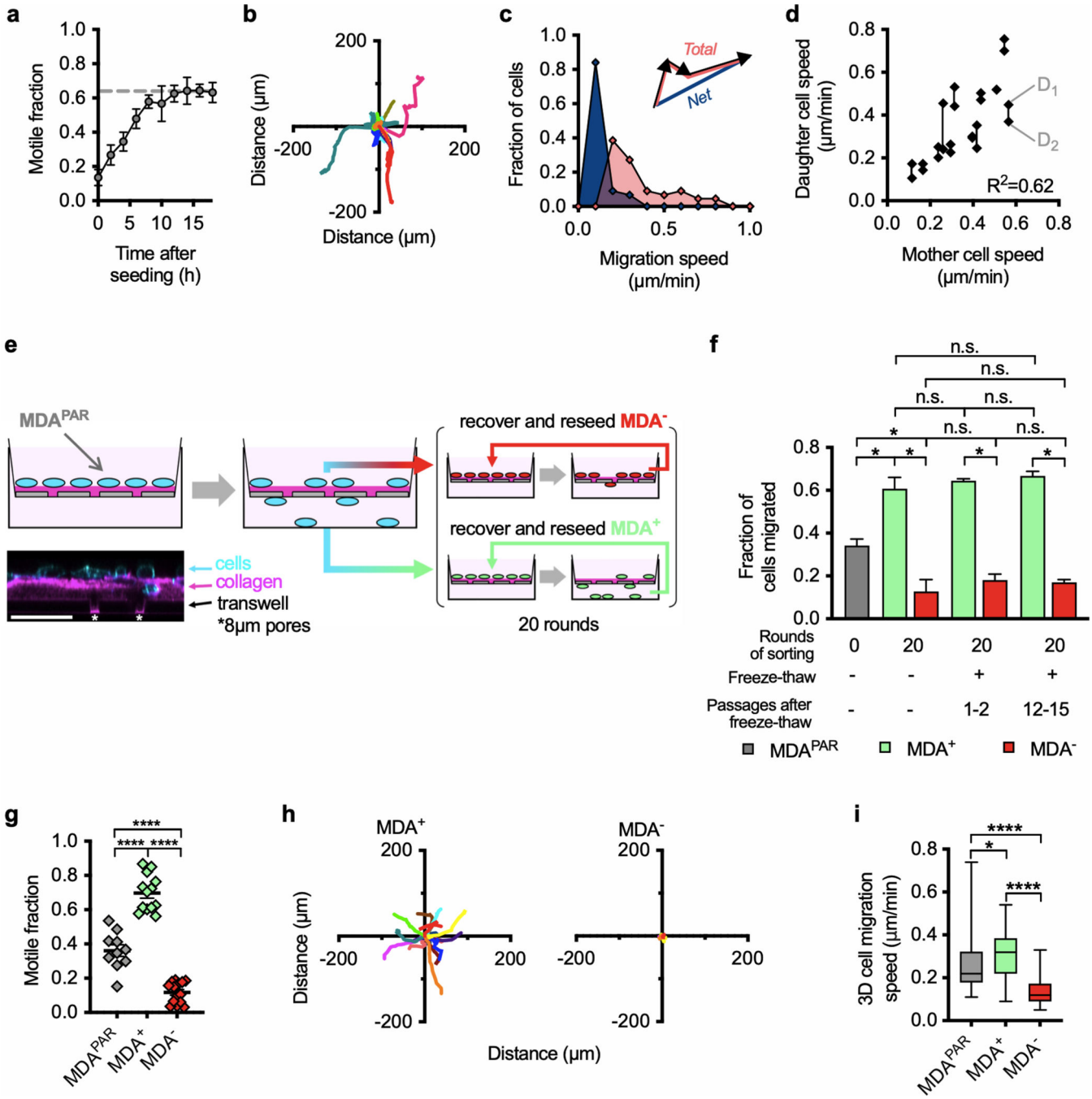

Figure 1.

Heterogeneity of MDA-MB-231 human cancer cell migratory capability is heritable and can be sorted based on migration behavior using an in vitro transwell migration assay. a) Fraction of motile MDA-MB-231 cells following seeding in 1.5 mg/mL collagen matrix. Dashed line indicates maximal motile fraction achieved by steady state. b) Single-cell migration paths and c) total and net cell migration speeds over 8 h. d) Correlation of total cell migration speed before and after mitosis. Each pair of daughter cells, D1 and D2, is connected by a vertical line, and the average daughter cell speed was used to determine

correlation (R^2 = 0.62). e) Schematic of migration cell sorting technique. f) Fraction of cells migrated through transwell assay for indicated populations after 4 days. g) Motile fraction of MDA-MB-231 subpopulations and parental cells. h) Single-cell migration paths of MDA-MB-231 subpopulations. i) Migration speeds of MDA-MB-231 subpopulations and MDA-MB-231 parental cells after seeding in 1.5 mg/mL collagen matrix. Data in (a), (f), and (g) display mean ± SEM. Statistical significance in (f) was calculated using one-way ANOVA (n = 3,4,4). Statistical significance in (g) was calculated using one-way ANOVA (n = 10,13,14). In (i), box and whisker plot show medians, 25^{th}/75^{th}, and minimum and maximum values. Statistical significance in (i) was calculated using a Kruskal-Wallis H test (n = 34,41,28). * $p < 0.05$, **** $p < 0.0001$, n.s., non-significant.

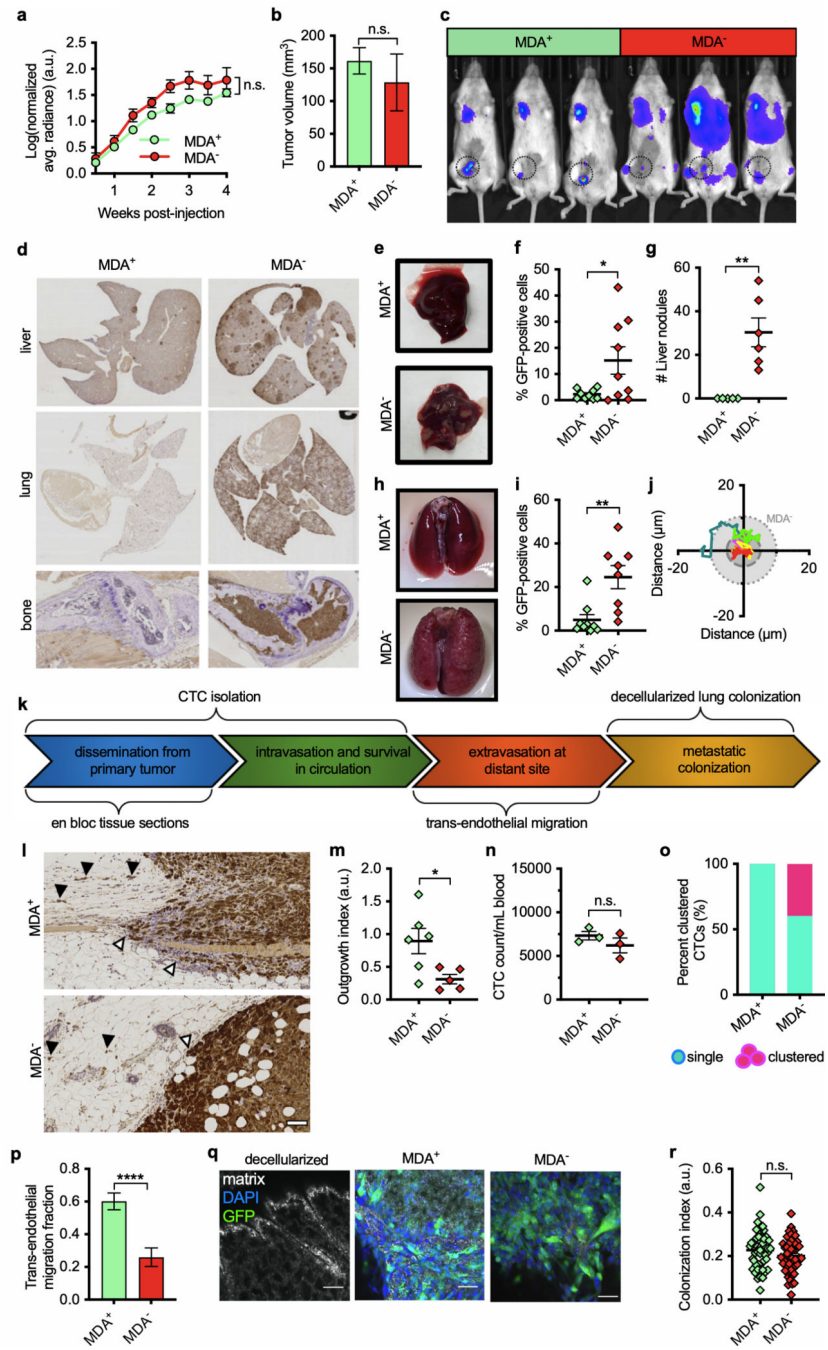

Figure 2.

Phenotypically sorted subpopulations show differential metastatic potentials in vivo. a) Primary tumor growth quantified by bioluminescence imaging using log(normalized average radiance) (n = 4). b) Primary tumor volume as measured by calipers (n = 3). c) Endpoint image showing metastasis via bioluminescence imaging. d) Representative images of anti-GFP immunohistochemical (IHC) staining of lung, liver, and bone samples counterstained with hematoxylin. e) Representative images of livers collected at study endpoint and f) quantification of percentage of GFP-positive cells in liver anti-GFP IHC sections (n = 9).

g) Quantification of metastatic liver nodules at study endpoint (n = 5,6). h) Representative images of lungs at study endpoint. i) Quantification of GFP-positive cells measured via IHC of lung histological sections (n = 8,9). j) Representative migration traces of MDA^- cells seeded in 1.5 mg/mL collagen after isolation from lungs of mice at 4 weeks post injection. Dark grey dashed line represents average distance migrated from MDA^- cells in vitro with light grey dotted line representing standard deviation. k) Schematic of stages of the metastatic cascade assessed by each experiment. l) Anti-GFP IHC staining of en bloc tumor sections; white arrow indicates local spread at the primary tumor periphery; black arrows indicate cell migration into the stroma. m) Quantification of outgrowth index to assess local dissemination in en bloc histology (n = 6,5). n) Quantification of circulating tumor cells (CTCs) per mL blood in orthotopically injected mice after 4 weeks (n = 3). o) Percentage of clustering of CTCs in mouse blood at 4 weeks (n = 3). p) Relative trans-endothelial migration fraction of MDA-MB-231 subpopulations (n = 3). q) Representative images of ex vivo lung decellularization colonization assay for MDA-MB-231 subpopulations imaged 9 d post-seeding using confocal reflectance and immunofluorescence; GFP-tagged cells: green, nuclei: blue, extracellular matrix: white; Scale bars: 50 μm. r) Quantification of colonization index in ex vivo lung tissue at 9 d post-seeding (n = 50). Data in (a), (b), (f), (g), (i), (m), (n), (p) and (r) display mean ± SEM. Statistical significance in (a) was calculated using multiple t-tests. Statistical significance in (b), (f), (g), (m), (n), (p) and (r) were calculated using unpaired, two-tailed Student t-tests. Statistical significance in (i) was calculated using a Mann-Whitney test. * $p < 0.05$, ** $p < 0.01$., **** $p < 0.0001$, n.s., non-significant.

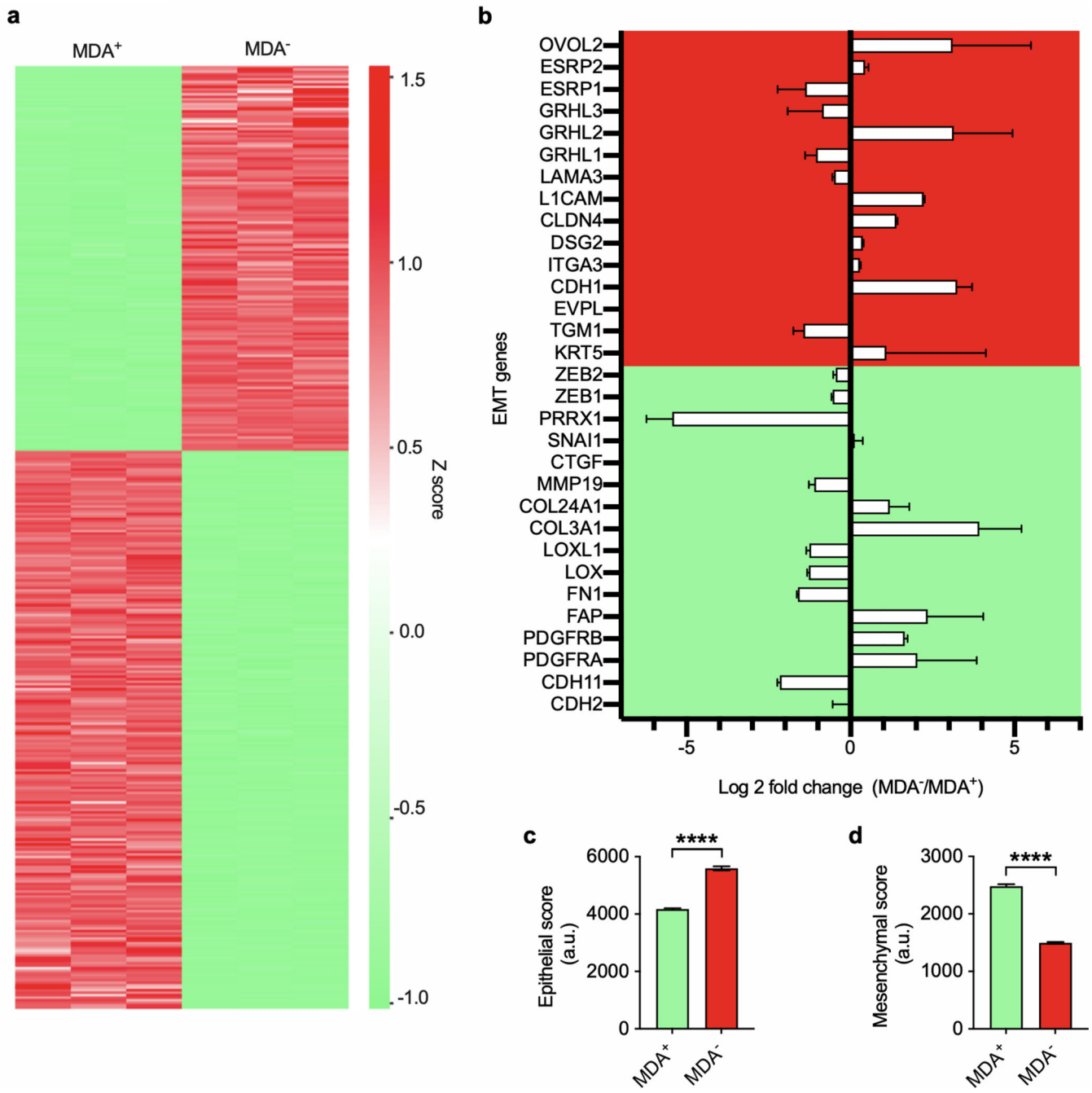

Figure 3.

RNA sequencing reveals differential EMT gene regulation in phenotypically sorted subpopulations. a) RNAseq Z score heatmap showing differential gene regulation of MDA^+ and MDA^- subpopulations (n = 3). b) Log 2 fold change of MDA^-/MDA^+ epithelial-to-mesenchymal transition genes (n = 3). c) Epithelial and d) mesenchymal scores for MDA^+ and MDA^- subpopulations (n = 3). Data in (b), (c), and (d) display mean ± SEM. Statistical significance in (c) and (d) was calculated using unpaired, two-tailed Student t-tests. **** $p < 0.0001$.

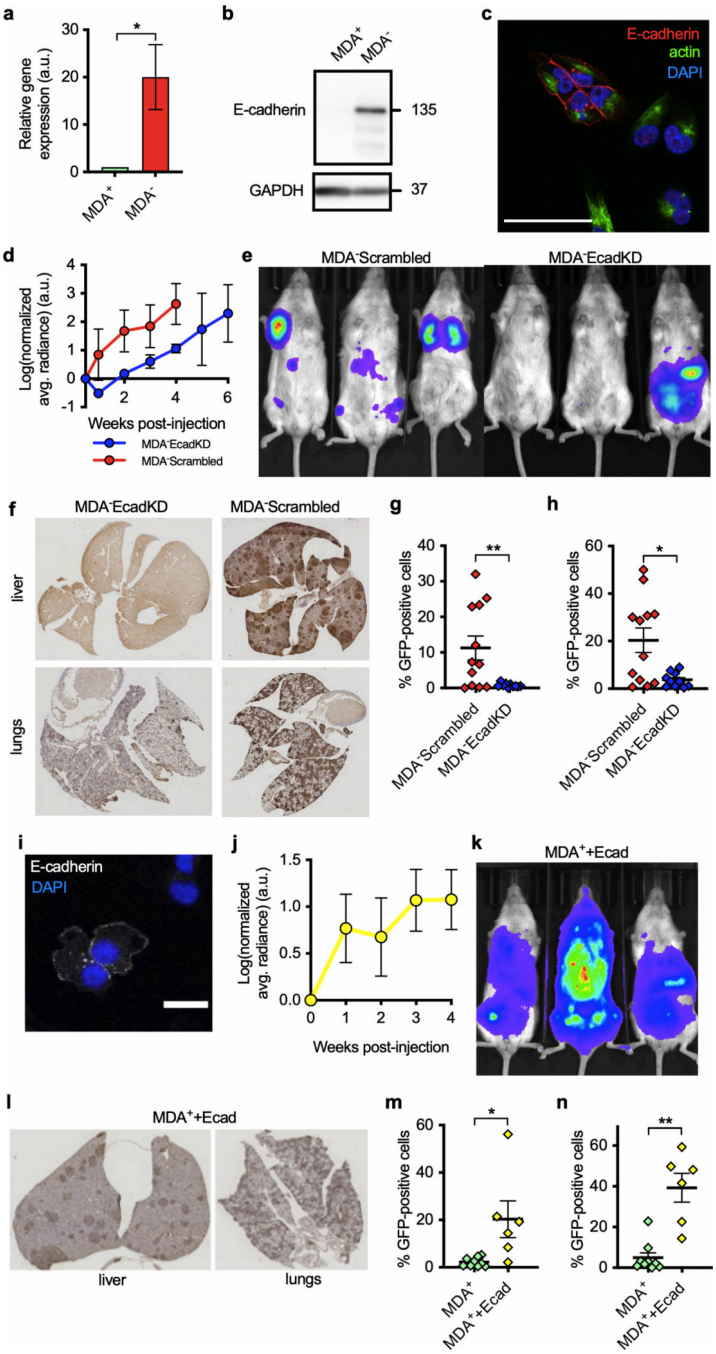

Figure 4.

E-cadherin expression is necessary for metastasis in phenotypically sorted subpopulations. a) qPCR of E-cadherin in MDA-MB-231 subpopulations normalized to MDA^+ cells (n = 3). b) Western blot of E-cadherin and GAPDH in subpopulations. c) Immunofluorescence staining of E-cadherin expression in MDA^- cells. Scale bar: 25 μm. d) Primary tumor growth of MDA^- E-cadherin knockdown and scrambled control tumors monitored via bioluminescence imaging (BLI) (n = 3). e) End point BLI of scrambled and E-cadherin knockdown mice at 4 weeks post tumor removal. f) Representative images of lung and

liver histological sections stained with anti-GFP IHC. Quantification of percentage of GFP-positive cells in g) liver (n = 10,12) and h) lung (n = 10,12) histological sections. i) Immunofluorescence staining of E-cadherin expression in MDA^+ + E-cadherin cells. Scale bar: 20 μm. j) Primary tumor growth of MDA^+ + E-cadherin tumors monitored via BLI (n = 6). k) End point BLI of MDA^+ + E-cadherin mice at 4 weeks post tumor removal l) Representative image of lungs and livers histological sections stained with anti-GFP IHC. Quantification of percentage of GFP-positive cells in m) liver (n = 6,9) and n) lung (n = 6,9) IHC-stained tissue sections. Data in (a), (d), (g), (h), (j), (m), and (n) display mean ± SEM. Statistical significance for (a), (g), and (h) was calculated using an unpaired, two-tailed Student's t-test. Statistical significance for (m) and (n) was calculated using a Mann-Whitney test. *$p < 0.05$, **$p < 0.01$.

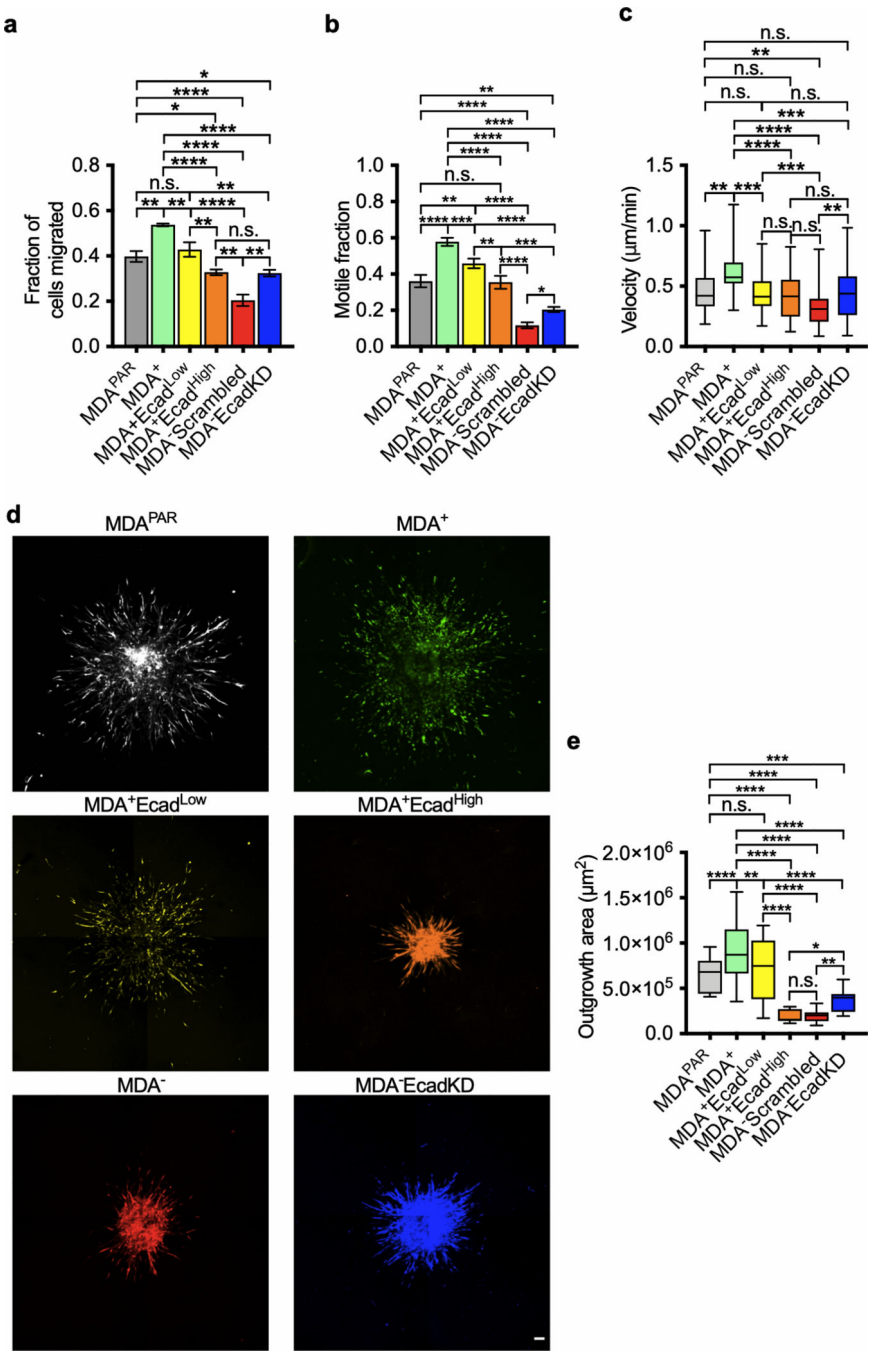

Figure 5.

E-cadherin expression tunes migration ability and mode in phenotypically sorted subpopulations. a) Fraction of cells migrated for MDA subpopulations with and without E-cadherin in transwell assays (n = 3). b) Motile fraction of MDA subpopulations with and without E-cadherin in 1.5mg/mL 3D collagen (n = 10–35). c) Microtrack migration speeds for MDA-MB-231 subpopulations with and without E-cadherin (n = 30–36). d) Representative images of tumor spheroid outgrowth at 48 h post-embedding. Scale bar: 100 μm e) Outgrowth area to quantify cell migration from in vitro tumor spheroids made from

MDA-MB-23 subpopulations with and without E-cadherin embedded in 1.5 mg/mL 3D collagen matrix at 48 h. Data from (a) and (b) display mean ± SEM. The box and whisker plot in (c) and (e) shows medians, $25^{th}/75^{th}$ percentiles, and minimum and maximum values. Statistical significance for (a) and (b) was calculated using an ordinary, one-way ANOVA. Statistical significance for (c) and (e) was calculated using a Kruskal Wallis H test. Statistical significance for (f) was calculated using an unpaired, two-tail Student's t-test. * $p < 0.05$, ** $p < 0.01$, *** $p < 0.001$, **** $p < 0.0001$, n.s., non-significant.

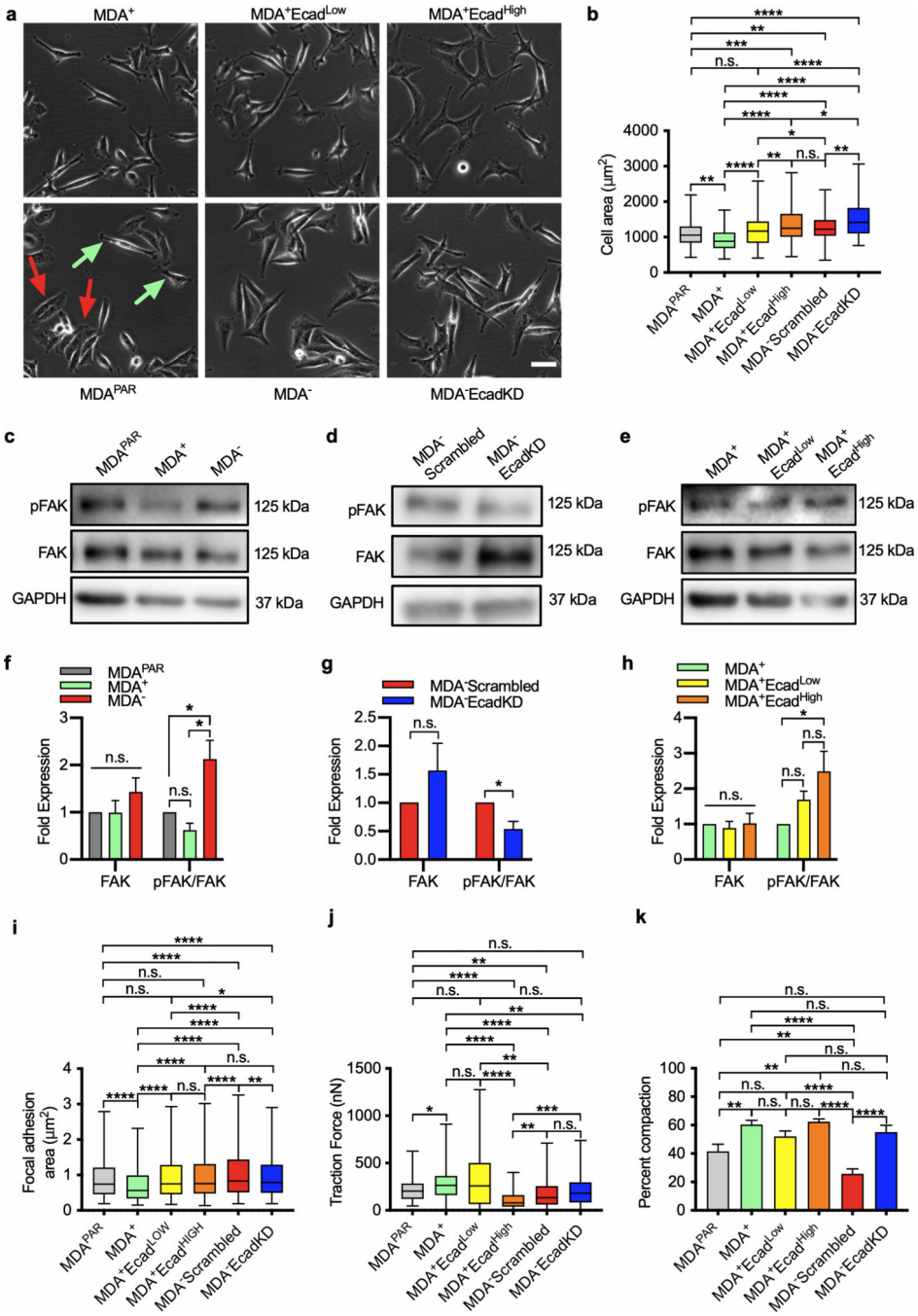

Figure 6.

Subpopulations exhibit differential morphologies, cell-ECM signaling, and contractility. a) Representative two-dimensional morphologies with red arrows pointing to parental cells with weakly motile-like morphologies and the green arrows pointing to parental cells with strongly motile-like morphologies; Scale bar: 50 μm. b) Quantification of cell area for subpopulations with and without E-cadherin. c) Western blot of pFAK, FAK, and GAPDH for MDA^{PAR}, MDA^{+}, and MDA^{-}. d) Western blot of pFAK, FAK, and GAPDH for MDA^{-} control and MDA^{-}EcadKD. e) Western blot of pFAK, FAK, and GAPDH for MDA^{+},

$MDA^{+}Ecad^{Low}$, and $MDA^{+}Ecad^{High}$. f) Quantification of FAK expression and activation from Western blot in (c) (n = 3). g) Quantification of FAK expression and activation from Western blot in (d) (n = 3). h) Quantification of FAK expression and activation from Western blot in (e) (n = 3). i) Quantification of focal adhesion area for subpopulations with and without E-cadherin. j) Total traction force magnitude, |F|, of MDA-MB-231 subpopulations with and without E-cadherin (n = 51–129). k) Percentage of bulk collagen matrix contraction for collagen gels seeded with MDA-MB-231 subpopulations with and without E-cadherin after 4 days (n = 4–14). Data from (f), (g), (h) and (k) display mean ± SEM. The box and whisker plots in (b), (i), and (j) shows medians, $25^{th}/75^{th}$ and minimum and maximum values. Statistical significance for (b), (i), and (j) were calculated using a Kruskal-Wallis H test. Statistical significance for (f), (h), and (k) were calculated using an ordinary, one-way ANOVA. Statistical significance for (g) was calculated using an unpaired, two-tailed Student's t-test. * $p < 0.05$, ** $p < 0.01$, *** $p < 0.001$, **** $p < 0.0001$, n.s. non-significant.

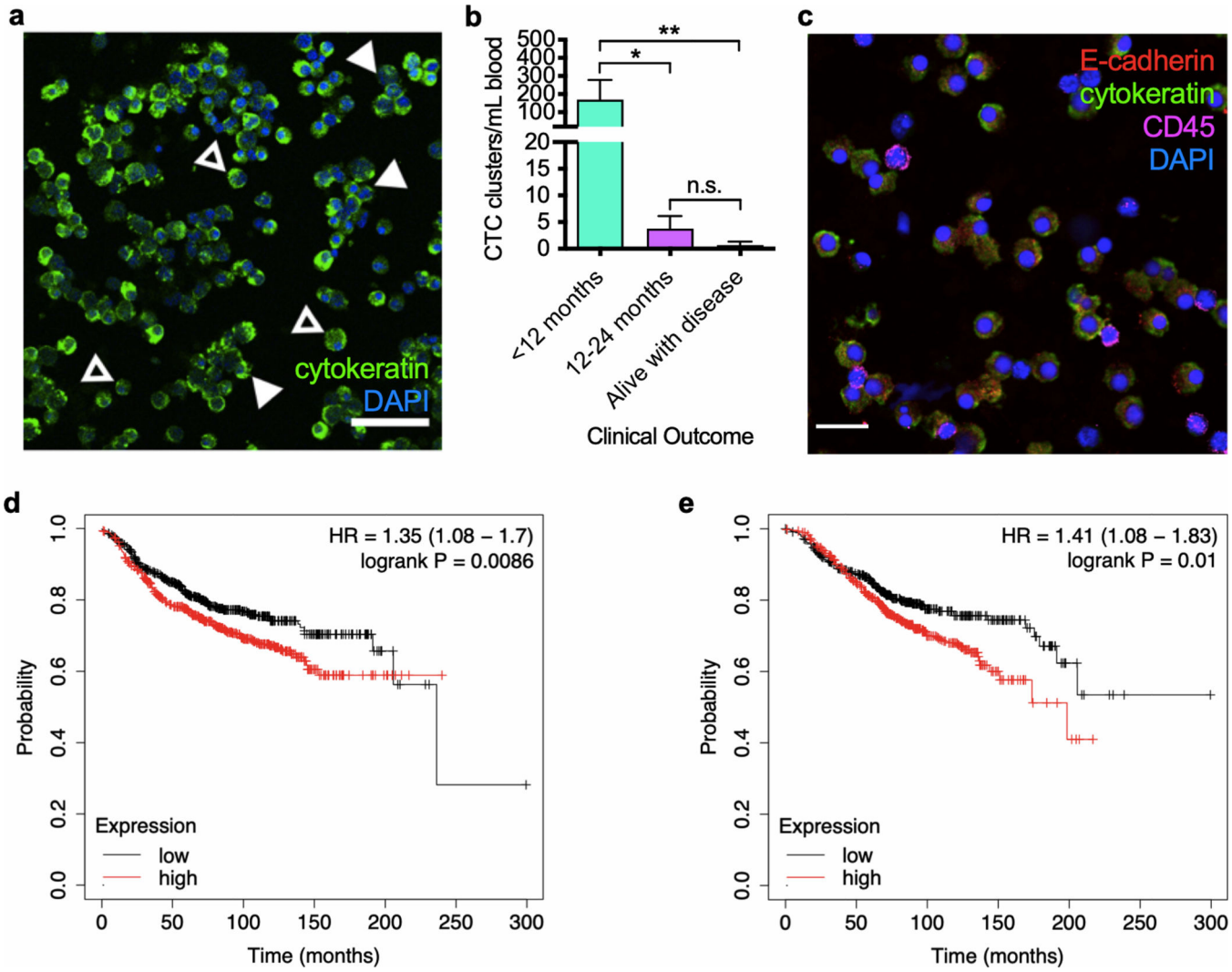

Figure 7.

Circulating tumor cell clusters and E-cadherin expression trend with worsened patient outcome. a) Representative image of circulating tumor cells (CTCs) from human cancer patient blood stained for cytokeratin (green) and DAPI (blue); filled arrows denote CTC clusters while empty arrows denote single CTCs. Scale bar: 50 μm. b) Quantification of CTC cluster concentration from blood isolated from 11 metastatic cancer patients binned by patient survival time. c) Representative image of CTCs isolated from metastatic breast cancer patient blood with E-cadherin (red), cytokeratin (green), CD45 (magenta), and DAPI (blue) staining. Scale bar: 20 μm. Kaplan-Meier curve depicting d) distal metastasis free survival (DMFS) and e) overall survival (OS) of upper and lower terciles of breast cancer patients divided by E-cadherin mRNA expression in the primary tumor. n = 1803 for (d) and n = 1402 for (e). Data in (b) display mean ± SEM. Significance was determined by a Kruskall-Wallis H test for (b). * $p < 0.05$, ** $p < 0.01$, n.s. non-significant.